Comparison of Electrical Characterization of AlGaN/GaN HEMT with Multi-finger Gate

Lijun He (helijun4@126.com)
Chongqing University of Posts and Telecommunications https://orcid.org/0000-0002-8255-6103
Boyang Zhao
Chongqing University of Posts and Telecommunications
Chengyun He
Chongqing University of Posts and Telecommunications
Zhiyang Xie
Chongqing University of Posts and Telecommunications
Xing Long
Chongqing University of Posts and Telecommunications
Zhaopeng Zhang
Chongqing University of Posts and Telecommunications
Fei Qi
Chongqing University of Posts and Telecommunications

Research Article

Keywords: AlGaN/GaN, TCAD, HEMT, RF, DC

Posted Date: August 31st, 2021

DOI: https://doi.org/10.21203/rs.3.rs-731171/v1

Abstract

This paper presents an exhaustive TCAD based comparison of the multi-gate and T-gate AlGaN/GaN HEMT. This paper simulates the DC and RF characteristics of the device and makes an accurate comparison. The important feature of the device such as threshold voltage, drain current output characteristics, transconductance, cut-off frequency, and maximum oscillation frequency were obtained. It is concluded that the shape optimization of the HEMT with multi-finger gates and the advantages over traditional T-gate devices. The device of two-finger gate with 50nm spacing has the best output characteristics, and its maximum saturation current is about 110% the size of the device of four-finger gate with 200nm at V_{GS}=0V. And the gm and the gain of the device with 50nm spacing two-finger gate is 76mS/mm larger than the HEMT of three-finger gate with 200nm. In addition, we also conducted a simulation in the case of changing only refers to finger-gate length and cap-gate length. And it is concluded that the two-finger gate HEMT with 250nm finger-gate length and 2.0μm cap-gate length has the best output characteristics, which output current is 0.159 $A/\mu m$ at V_{GS}=-1.5V. The results show that AlGaN/GaN HEMT with multi-finger gate have great potential for high power and high frequency applications electronic devices.

1 Introduction

GaN-based materials mainly include AlGaN, GaN, InAlN and AlN. In the application of electronic devices, GaN material has the characteristics of high breakdown field strength and high electron mobility compared with the previous two generations of semiconductors, which makes it have great advantages in the field of high frequency and high power [1–3]. The band gap of gallium nitride is 3.4eV, which is 2eV higher than Si and GaAs, which ensures that the device can work normally in a radiation environment without failure; third-generation semiconductor materials such as gallium nitride and silicon carbide strike [4–7]. Compared with Si and GaAs, the breakdown field of the third-generation semiconductor materials such as GaN and SiC is one order of magnitude higher [8]. In the same size, the breakdown voltage of GaN and SiC devices is one order of magnitude higher than that of Si and GaAs devices, ensuring the high-power output of the device [9–12]. Because SiC lacks a heterojunction structure, the device structure mainly uses metal semiconductor field effect transistors, and field effect transistors are surface devices, the carrier transport is affected by the surface, resulting in low mobility, which limits the devices in the high-frequency field applications. Compared with SiC materials, GaN materials also have the advantage of adjustable composition, so that semiconductor materials with different band gap can be obtained by adjusting the composition, and materials with different band gap are combined to form a heterojunction [13–17]. GaN material has a wurtzite structure, which has strong spontaneous polarization and piezoelectric polarization effect, which makes two-dimensional electron gas form at the heterogeneous interface, so the heterojunction material has excellent current control ability and high electron migration. HEMT is made based on heterojunction materials [18–20]. Due to the reduced scattering of ionized impurities, the mobility of GaN-based HEMT is much higher than that of SiC field effect transistors, so GaN-based HEMT is suitable for making microwave and millimeter-wave power amplifiers [21–23].

A lot of research has been conducted on GaN-based HEMTs, mainly focusing on improving the f_T, VBR, and power added efficiency. So far, various parameters of AlGaN/GaN HEMT have been studied in detail, and some modifications have been made, including adding and optimizing the length of the field strength plate, the lateral misalignment of the field plate, floating gate, and different passivation layer, gate insulation, the introduction of GaN cap layer, etc. In this paper, the influence of multi-finger gates on the performance of HEMT is studied. All performance studies are carried out using the TCAD tool ATLAS.

2 Device Structure

In this study, Multi-finger gate AlGaN/GaN HEMT has been implemented. In this paper, we change the shape and parameters of the multi-finger gate. We have designed three types of multi-finger gates, which are two-finger, three-finger, and four-finger types. The multi-finger gate is composed of the finger gate and the cap-gate, the finger gate is on the bottom, and the cap-gate is on the top. We designed the parameters of the device and got the DC and RF capabilities of the cross-sectional schematic of T-gate, and two-finger gate, three-finger gate, and four-finger gate AlGaN/GaN HEMT analyzed in this paper are presented in Fig. 1, where the parameters of layers and electrodes details are given. The AlGaN/GaN epitaxial layers have been grown on sapphire substrate, the epilayer consisted of, from bottom to top, $1\mu m$ GaN buffer layer, $473.3nm$ unintentionally doped (UID) GaN spacer layer, $26.7nm$ AlGaN barrier layer that mole fraction of Al is 0.25, and a Si_3N_4 passivate layer. The length of drain and source is$1\mu m$ and $3\mu m$, respectively. The length of gate is $600nm$. The length of each type of multi-finger gate is halved by $600nm$, and the spacing between two adjacent finger gates is equal. All simulations are based on the above AlGaN/GaN HEMT epilayers structure.

3 Simulation Model

In this study, we have completed the simulation and optimization of AlGaN/GaN HEMT based on Silvaco. Perform device simulations by combining models such as SRH recombination. The polarization model is also included. Then perform a detailed simulation to calibrate the simulation results based on the data reported in the experiment. For the simulation of GaN-based HEMT devices, the setting of the polarization model is overly critical, which is related to the generation of 2DEG. In the simulation model, we use the polarization model to automatically calculate the polarization. We can declare the POLAR.SCALE parameter in the simulation to change the sign and magnitude of the charge in the material. The default value of the POLAR.SCALE parameter is 1.0. In this simulation, we set the value to 0.75. Device simulation software ATLAS mainly uses mathematical models such as the Poisson equation and continuity equation to solve the characteristic parameters of the simulated device. As the gate length decreases, the electric field intensity in the channel under the gate is exceptionally large, and the carriers in the channel will produce velocity saturation effects, so the GANSAT.N high field mobility model in the simulation software is adopted. When simulating the frequency characteristics, we used the lattice self-heating model LAT.TEMP.

4 Results And Discussions

In this section, we study the effects of different multi-finger gates on the device according to output characteristics, transfer characteristics, extrinsic transconductance (g_m), current gain cut-off frequency (f_T) and maximum oscillation frequency(f_{max}). In this section, we change the number of branches of the multi-finger gate and the distance between adjacent branches to observe and analyze the changes in device performance.

The output characteristics of devices with different multi-finger gates are shown in Fig. 2. By sweeping the gate voltage V_{GS} between − 1.5*V* to 0 in a step of 0.5*V*, and V_{DS} is in the range from 0 to 15*V*. Figure 2a is the output curve of a two-finger gate device with different spacing. The HEMT with two-finger gate with 50*nm* spacing has the maximum saturation current is about 0.246*A/μm* at V_{DS}=15*V* and V_{GS}=0*V*. The drain current of HEMT of two-finger gate with 200*nm* spacing is smallest which is 0.233 *A/μm*. And HEMT of two-finger gate with 100*nm* spacing and 150*nm* is almost the same that is about 0.242*A/μm* at V_{DS}=15*V* and V_{GS}=0*V*. In Fig. 2b, result of drain current of the HEMT with three-finger gate are plotted. The I_D-V_{DS} curves of three-finger gate devices with a 50*nm* and 150nm spacing curve basically coincides and has the largest saturated output current 0.236*A/μm*. Secondly, the saturation current of the device of three-finger gate devices with a 100*nm* spacing is slightly smaller, which is 0.230*A/μm*. The maximum drain current of the device of three-finger gate devices with a 200*nm* spacing is still the smallest. Figure 2c also exhibits a maximum drain of 0.239*A/μm* output current when the finger spacing of the four-finger gate device is 50*nm*. And the drain current of HEMT of four-finger gate with 200*nm* spacing is smallest which is 0.227*A/μm*. Among the output characteristics of all devices, the two-finger gate device has the largest output characteristics, and the saturation drain current of the two-finger gate device with a spacing of 50nm is the largest.

The dc transfer characteristics are exhibited in Fig. 3. The gate was biased from − 10*V* to 2*V* in a step of 0.25*V* and the drain was biased at 5*V*. It can be observed from Fig. 3a that, the threshold voltage of the devices' two-finger gate with 50*nm* and 200*nm* spacing is the same, the V_{TH}=-4.9*V*. The threshold voltage of the devices' two-finger gate with 50nm and 200nm spacing is the same, the V_{TH}=-4.7*V*. Figure 3b exhibits that the threshold voltage of the multi-finger gate device from small to large corresponds to the multi-finger gate spacing of 150*nm*, 50*nm*, 200*nm*, 100*nm*, respectively. The threshold voltage of the four-finger gate devices was plotted in Fig. 3c. the threshold voltage of the devices' finger-gate with 100*nm* and 200*nm* spacing is the same, the V_{TH}=-5.1*V*. Then, the 50*nm* spacing device has a V_{TH} of -5.0*V*, and the 150*nm* spacing device has a V_{TH} of -4.8*V*. In summary, the two-finger gate device with 50*nm* and 200*nm* spacing are most positively shifted. The Fig. 4 manifests that among all multi-finger gate devices, transconductance refers to the ratio of the change value of the output current to the change value of the input voltage. The capabilities of the gate to control the channel current is related to the value of g_m. The larger the g_m, the better the capabilities to control the current. Figure 4a plots the curve of device with two-finger gate, when the transconductance of the four devices achieve the peak. Device with 50*nm* and 100*nm* spacing has maximum g_m of 484*mS/mm* at V_{TH}=-1.75*V*. Two-finger gate device with 150*nm*

spacing have a transconductance of 468*mS/mm*. Device with 200*nm* spacing have a minimum value among the four devices, the g_m is 432*mS/mm*. The curve of device with three-finger gate be exhibited in Fig. 4b. In Fig. 4b Device with 50*nm* spacing has a maximum g_m that is 472*mS/mm* at V_{TH}=-1.75*V*. The g_m of device with 100*nm* and 150*nm* are approximate which are about 465*mS/mm*. But the gate voltages when they obtain the maximum transconductance are different. Device with 200*nm* spacing still have a minimum value among the four devices, the g_m is 408*mS/mm*. Figure 4c exhibits that the g_m of the curve of device with four-finger gate. Device with 50*nm* spacing has maximum g_m of 481*mS/mm* at V_{TH}=-1.75*V*. When the multi-finger spacing is 100*nm*, 150*nm* and 200*nm*, respectively. The devices' g_m is 462*mS/mm* 458*mS/mm* and 449*mS/mm*, respectively. It can be seen that the g_m of the device will become smaller as the distance between the multi-finger gates decreases.

Figure 5 shows the RF characteristics of the device, including the variation of the h_{21} and the MSG curve with frequency. From Fig. 5, there is a little difference between f_T and f_{max}. because the length of gate of device has not changed. The f_T of the device is about 7GHz, and the f_{max} is about 65GHz. However, with the change of gate shape, the current gain(h_{21}) and maximum stable gain(MSG) of the device change obviously. It can be observed from the three figures that the device with a 50*nm* spacing finger-gate has the largest MSG. And the h_{21} of the two-finger, three-finger, four-finger gate devices are greater than that of the T-gate device. The h_{21} of the two-finger, three-finger, and four-finger gate devices with a 50*nm* spacing finger-gate is 132.1*dB*, 133.7*dB*, and 140.9*dB*, respectively. But for MSG, the device of two-finger gate with 150*nm* has MSG of 76.3*dB*, the MSG three-finger gate with 50*nm* is 75.9*dB*, and four-finger gate with 100*nm* has 79.5*dB* MSG.

After then, we set the spacing of the two-finger gate at 50nm spacing and changed the length of each finger gate to obtain the DC characteristics of different multi-finger gate lengths. Figure 6 presents the DC performance of the AlGaN/GaN HEMT with different multi-finger gate lengths, including output characteristics, transfer characteristics and transconductance. Figure 6a presents the output characteristics of the device at V_{GS}=-1.5*V*. It can be observed from the figure that as the gate length of the device decreases, the maximum saturation current of the device will increase, but as the gate length is further reduced, the device will have short Channel effect, manifested as the phenomenon of output current not being saturated. It can also be observed from the figure that when the finger gate length is reduced to 250nm, the maximum saturation current is 0.159 *A/μm*, and there is no current unsaturation phenomenon. Figure 6b shows the transmission characteristics of the device. It can be seen from the figure that as the length of each multi-finger gate of the device is from 350*nm* to 50*nm*, the threshold voltage will shift to negative. The peak transconductance of device be plotted in Fig. 6c. It can be observed from the figure that as the gate length of the device decreases, the peak transconductance of HEMT will increase. When the finger gate length of the device is reduced to 50nm, it has the largest maximum transconductance, and the value of g_m is 570*mS/mm*.

Figure 7 shows the changes in the output characteristics, transfer characteristics and transconductance of the device with the cap-gate length changed when the finger-gate length is set to 250*nm*. Figure 7a

shows the output characteristics of the device at V_{GS}=-1.5*V*. It can be seen from the Fig. 7a that when the cap-gate length of the device is reduced, the maximum saturation current of the device will become larger and tend to be the same. However, as the length of the cap-gate decreases, the output current of the device will also become unsaturated. The transfer characteristics of the device shown in Fig. 7b show the change in the length of the cap-gate, which hardly affects the threshold voltage of the device. From Fig. 7c, the maximum transconductance of device is less affected by cap-gate changes length. When device have a 1.4μm cap-gate length, the g_m of device has a maximum value that is 509*mS/mm*. The device has the smallest gm of 491*mS/mm* when the cap-gate length is 2.0μm.

5 Conclusion

In this study, we compare HEMT devices with multi-finger gates and T-gate devices and get the difference in DC and RF characteristics. And there is a significant gap between DC and RF characteristics. When the multi-finger gate device has the same number of finger-gate, and the distance between the finger-gate is 50*nm*, it has the maximum saturation current. The threshold voltage of the device will first shift to positive and negative shift as the finger-gate spacing increases. The influence of the number and spacing of the finger gates on the RF characteristics is mainly reflected in the change of the gain, and the h_{21} and the MSG of devices are larger than the traditional T-shaped gate. Finally, we simulated a variety of devices that only changed the length of the finger gate and the cap-gate length and obtained the optimal situation of the two-finger gate device, which is the two-finger gate HEMT with 250*nm* finger-gate length and 2.0μm cap-gate length.

6. Declarations

Conflict of interest

The authors declare that they have no conflict of interest.

Acknowledgments

This work was supported by the China Scholarship Council Study Program for Young Backbone Teachers under grant no. 201707845017, the National Nature Science Foundation of China under grant no. 61804020, the Scientific and Technological Research Foundation of Chongqing Municipal Education Commission under grant no. KJQN201900643 and no. KJQN202000646, the Chongqing Natural Science Foundation of Chongqing Municipal Science and Technology Bureau under grant no. cstc2020jcyj-msxmX0550, the Raised Fund Plan of National Natural Science Foundation of China of Chongqing University of Posts and Telecommunications grant no. A2016-143 and no. A2020-528, the PhD scientific research foundation of Chongqing University of Posts and Telecommunications under grant no. A2015-11 and no. A2015-12.

Availability of data

The datasets used or analyzed during the current study are available from the corresponding author on reasonable request.

7. References

1. Chung, J. W., Hoke, W. E., Chumbes, E. M., Palacios, T.: AlGaN/GaN HEMT With 300-GHz f_{max}. IEEE Electron Device Letters **31(3)**, 195-197 (2010). https://doi.org/10.1109/LED.2009.2038935

2. Kumar, V., Kuliev, A., Schwindt, R., Muir, M., Simin, G., Yang, J., Asif Khan, M., Adesida, I.: High performance 0.25 μm gate-length AlGaN/GaN HEMTs on sapphire with power density of over 4.5 W/mm at 20 GHz. Solid-State Electronics **47(9)**, 1577-1580 (2003). https://doi.org/10.1016/S0038-1101(03)00078-9

3. Efthymiou, L., Longobardi, G., Camuso, G., Chien, T., Chen, M., Udrea, F.: On the physical operation and optimization of the p-GaN gate in normally-off GaN HEMT devices. Applied Physics Letters **110(12)**, 123502 (2017). https://doi.org/10.1063/1.4978690

4. Zhang, X., Wang, L., Li, W., Tao, L., Chen, X.: Gallium Nitride Dual Two-Dimensional Electron Gas HEMT with a Good Performance: Based on TCAD simulations. 2020 21st International Conference on Electronic Packaging Technology (ICEPT). IEEE, 1-4 (2020). https://doi.org/10.1109/ICEPT50128.2020.9202882

5. Choi, Y. C., Pophristic, M., Cha, H. Y., Peres, B., Spencer, M.G., Eastman, L. F.: The effect of an Fe-doped GaN buffer on off-state breakdown characteristics in AlGaN/GaN HEMTs on Si substrate. IEEE transactions on Electron devices **53(12)**, 2926-2931 (2006). https://doi.org/10.1109/TED.2006.885679

6. Zine-eddine, T., Zahra, H., Zitouni, M.: Design and analysis of 10 nm T-gate enhancement-mode MOS-HEMT for high power microwave applications. Journal of Science: Advanced Materials and Devices **4(1)**, 180-187 (2019). https://doi.org/10.1016/j.jsamd.2019.01.001

7. Hasan, M. R., Motayed, A., Fahad, M. S., Rao, M. V.: Fabrication and comparative study of DC and low frequency noise characterization of GaN/AlGaN based MOS-HEMT and HEMT. Journal of Vacuum Science & Technology B, Nanotechnology and Microelectronics **35(5)**, 052202 (2017). https://doi.org/10.1116/1.4998937

8. Visalli, D., Van Hove, M., Srivastava, P., Derluyn, J., Das, J., Leys, M., Degroote, S., Cheng, K., Germain, M., Borghs, G.: Experimental and simulation study of breakdown voltage enhancement of AlGaN/GaN heterostructures by Si substrate removal. Applied Physics Letters **97(11)**, 113501 (2010). https://doi.org/10.1063/1.3488024

9. Clymore, C. J., Mohanty, S., Jian, Z. A., Krishna, A., Keller, S., Ahmadi, E.: HfO_2 as gate insulator on N-polar GaN-AlGaN heterostructures. Semiconductor Science and Technology **36(3)**, 035017 (2021). https://doi.org/10.1088/1361-6641/abe21c

10. Sehra, K., Kumari, V., Gupta, M., Mishra, M., Rawal, D. S., Saxena, M.: TCAD Investigation of Gate-Lag Measurements on Conventional and π-Gate AlGaN/GaN HEMTs. 2020 IEEE 20th International Conference on Nanotechnology (IEEE-NANO). IEEE, 128-133 (2020). https://doi.org/10.1109/NANO47656.2020.9183484

11. Heikman, S., Keller, S., Wu, Y., Speck, J. S., Denbaars, S. P., Mishra, U. K.: Polarization effects in AlGaN/GaN and GaN/AlGaN/GaN heterostructures. Journal of applied physics **93(12)**, 10114-10118 (2003). https://doi.org/10.1063/1.1577222

12. Chen, K. J., Zhou, C.: Enhancement-mode AlGaN/GaN HEMT and MIS-HEMT technology. physica status solidi (a) **208(2)**, 434-438 (2011). https://doi.org/10.1002/pssa.201000631

13. Amit, M., Rawal, D. S., Sharma, S., Kapoor, S., Liashram, R., Chaubey, R. K., Vinayak, S., Sharma, R. K.: Design and fabrication of multi-finger field plate for enhancement of AlGaN/GaN HEMT breakdown voltage. Defence Science Journal **68(3)**, 290-294 (2018). https://doi.org/10.14429/dsj.68.12134

14. Latorre Rey, A. D., Albrecht, J. D., Saraniti, M.: A Π-Shaped Gate Design for Reducing Hot-Electron Generation in GaN HEMTs. IEEE Transactions on Electron Devices **65(10)**, 4263-4270 (2018). https://doi.org/10.1109/TED.2018.2863746

15. Colangeli, S., Giofrè, R., Ciccognani, W., Limiti, E.: A multi-finger modeling approach to correctly predict the inherent stability of a custom active device. 2017 IEEE MTT-S International Microwave Symposium (IMS). IEEE, 1784-1786 (2017). https://doi.org/10.1109/MWSYM.2017.8058994

16. Sehra, K., Kumari, V., Nath, V., Gupta, M., Saxena, M.: Optimization of Asymmetric π Gate HEMT for Improved Reliability & Frequency Applications. 2019 IEEE 9th International Nanoelectronics Conferences (INEC). IEEE, 1-4 (2019). https://doi.org/10.1109/INEC.2019.8853857

17. Su, L. Y., Lee, F., Huang, J. J.: Enhancement-mode GaN-based high-electron mobility transistors on the Si substrate with a P-type GaN cap layer. IEEE Transactions on Electron Devices **61(2)**, 460-465 (2014). https://doi.org/10.1109/TED.2013.2294337

18. Martinez, P. J,, Letz, S., Maset, E., Zhao, D.: Failure analysis of normally-off GaN HEMTs under avalanche conditions. Semiconductor Science and Technology **35(3)**, 035007 (2020). https://doi.org/10.1088/1361-6641/ab6bad

19. Yamaguchi, R., Suzuki, Y., Asubar, J. T., Tokuda, H., Kuzuhara M.: Reduced current collapse in multi-fingered AlGaN/GaN MOS-HEMTs with dual field plate. 2017 IEEE International Meeting for Future of Electron Devices, Kansai (IMFEDK). IEEE, 92-93 (2017). https://doi.org/10.1109/IMFEDK.2017.7998058

20. Saadaoui, S., Fathallah, O., Maaref, H.: Effects of current transportation and deep traps on leakage current and capacitance hysteresis of AlGaN/GaN HEMT. Materials Science in Semiconductor Processing **115**, 105100 (2020). https://doi.org/10.1016/j.mssp.2020.105100

21. Sehra, K., Kumari, V., Gupta, M., Mishra, M. Rawal, D. S.,Saxena, M.: Optimization of π−Gate AlGaN/AlN/GaN HEMTs for Low Noise and High Gain Applications. Silicon, 1-12 (2020). https://doi.org/10.1007/s12633-020-00805-7

22. Uren, M. J., Moreke, J., Kuball, M.: Buffer design to minimize current collapse in GaN/AlGaN HFETs. IEEE Transactions on Electron Devices **59(12)**, 3327-3333 (2012). https://doi.org/10.1109/TED.2012.2216535

23. Hontz, M. R,, Chu, R., Khanna, R.: TCAD modeling of a lateral GaN HEMT using empirical data. 2018 IEEE Applied Power Electronics Conference and Exposition (APEC). IEEE, 244-248 (2018). https://doi.org/10.1109/APEC.2018.8341017

Figures

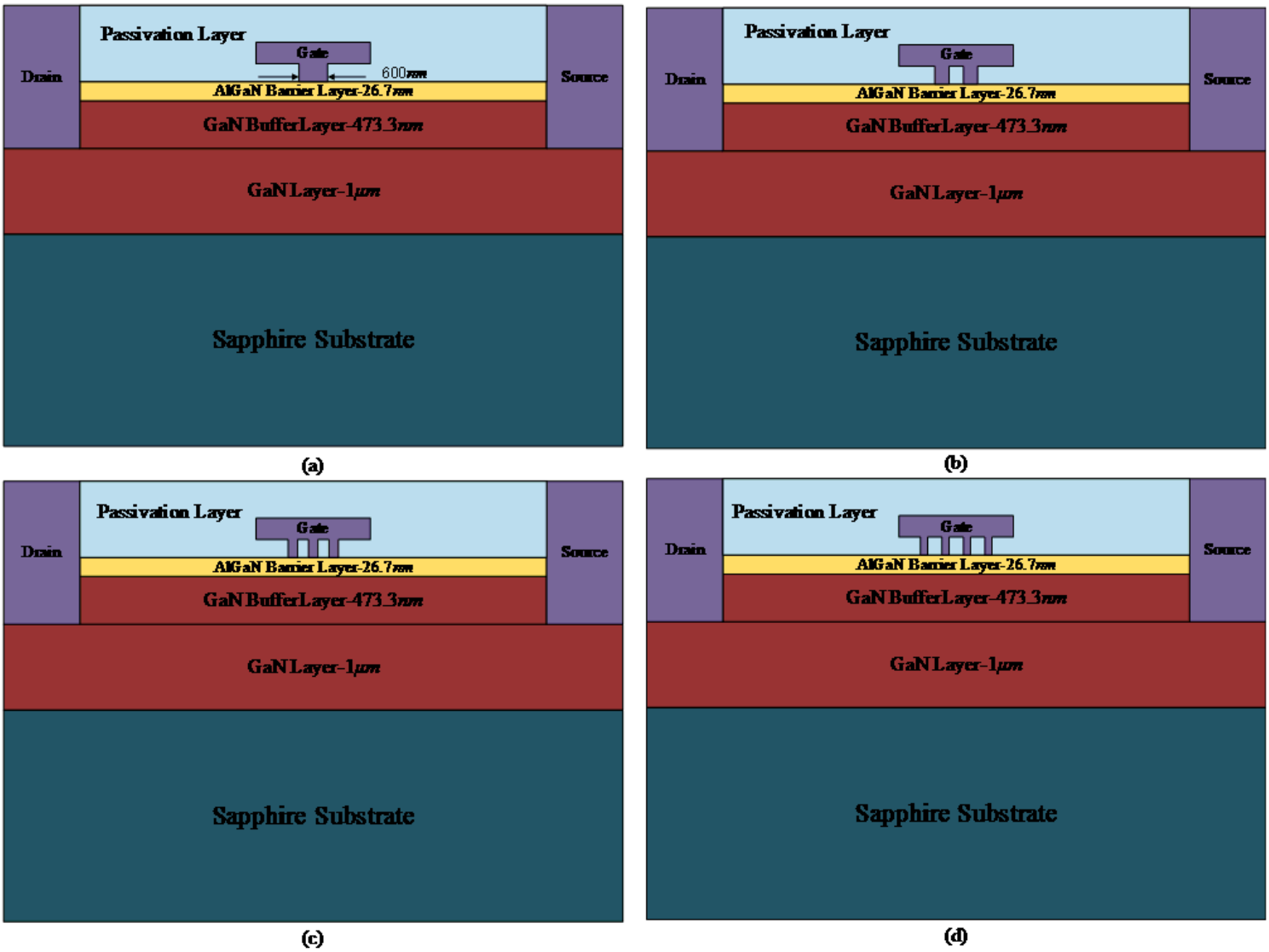

Figure 1

a T-shape gate AlGaN/GaN HEMT. b Two-finger gate AlGaN/GaN HEMT. c Three-finger gate AlGaN/GaN HEMT. d Four-finger gate AlGaN/GaN HEMT

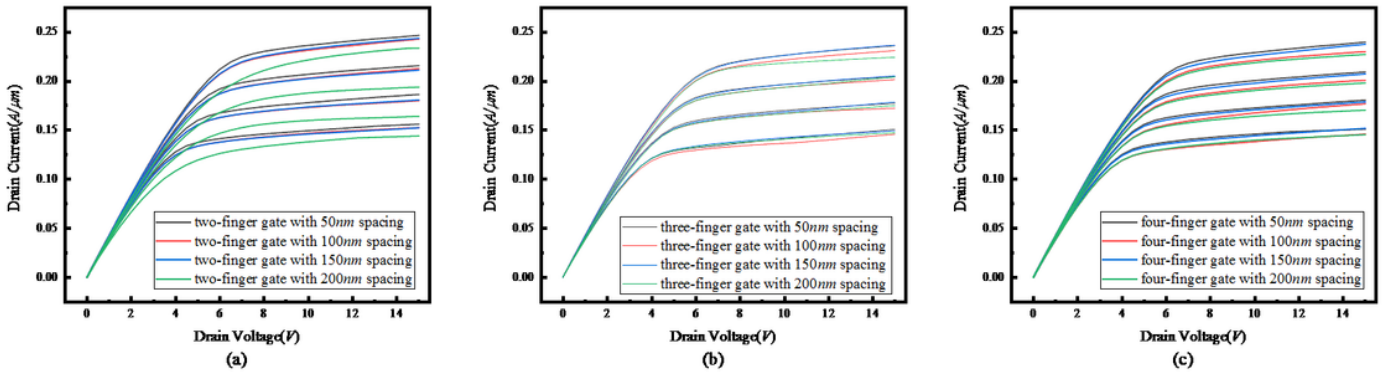

Figure 2

Output characteristics curve or ID-VDS plots at VGS from -1.5V to 0 a two-finger gate, b three-finger gate, c four-finger gate

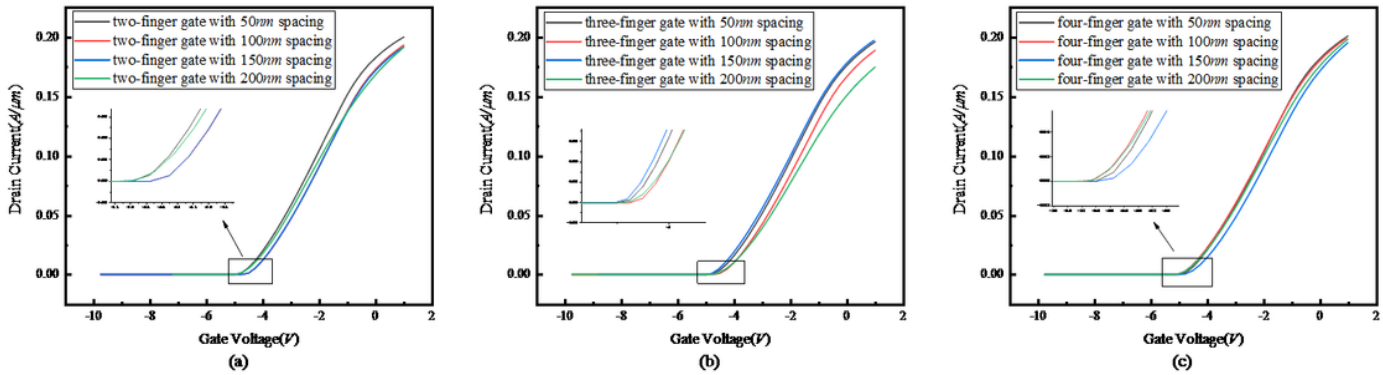

Figure 3

Transfer characteristics curve or ID-VGS plots at VDS=5V a two-finger gate, b three-finger gate, c four-finger gate

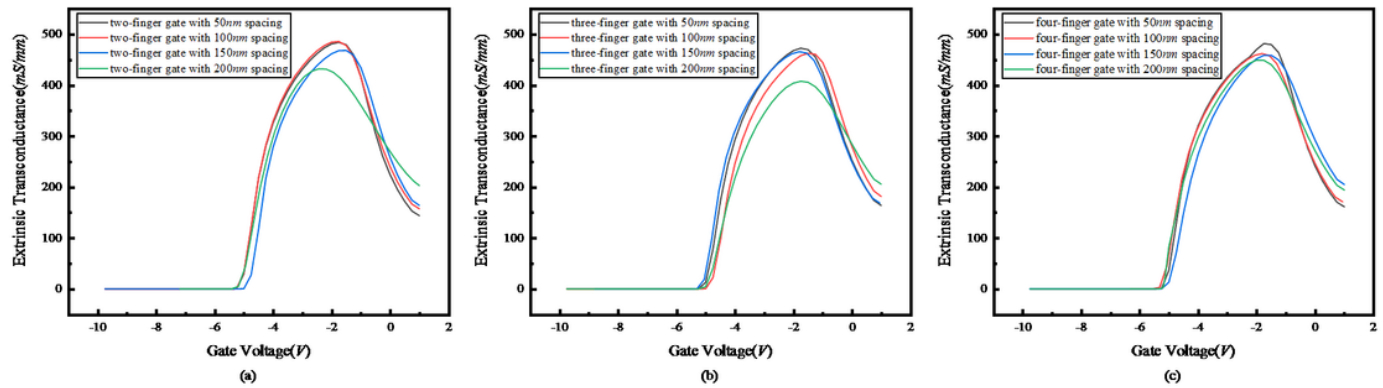

Figure 4

Transconductance(gm) curve plots at VDS=5V a two-finger gate, b three-finger gate, c four-finger gate

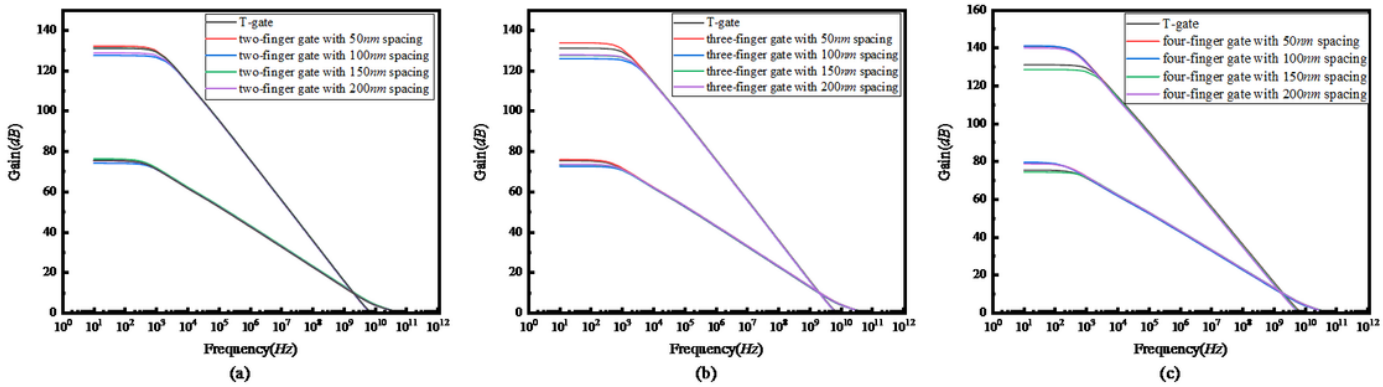

Figure 5

h21 and MSG curve of device a two-finger gate, b three-finger gate, c four-finger gate

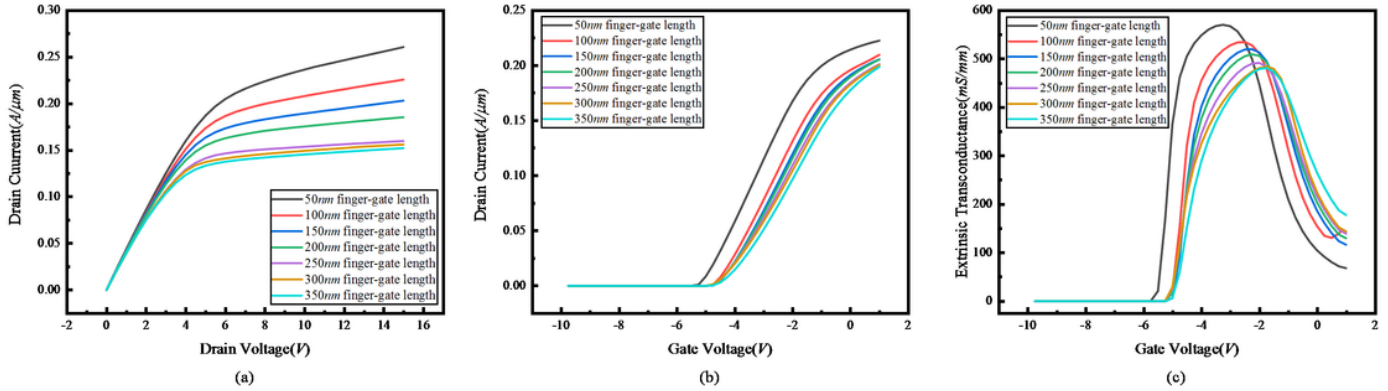

Figure 6

DC performance of the AlGaN/GaN HEMT with different multi-finger gate lengths a Output characteristics curve, b Transfer characteristics curve, c Transconductance(gm) curve

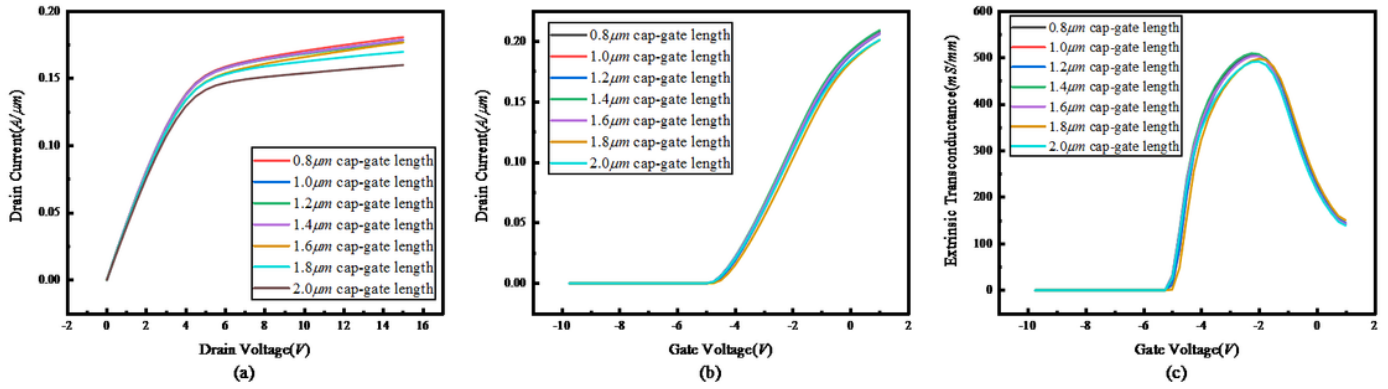

Figure 7

DC performance of the AlGaN/GaN HEMT with different cap-gate lengths a Output characteristics curve, b Transfer characteristics curve, c Transconductance(gm) curve